Experimental and Theoretical Study of Pentaerythritol Tetranitrate Conformers

Yuri A. Gruzdkov, Zbigniew A. Dreger,* and Yogendra M. Gupta

Institute for Shock Physics and Department of Physics, Washington State University, Pullman, Washington 99164-2816

Received: March 15, 2004

Raman measurements and density functional theory (DFT) calculations were carried out to evaluate the propensity of pentaerythritol tetranitrate (PETN) to conformational changes. In the crystalline phase under ambient conditions, the PETN molecule has S_4 symmetry. Two instances of symmetry change were found and presented in this work. One involved compressing the PETN crystal statically to ≥ 5 GPa in a diamond anvil cell. The other was observed upon dissolving PETN in a polar solvent (acetone-d_6). DFT calculations indicate that changes in conformation/symmetry can be observed readily through changes in the vibrational spectrum. Several representative stable PETN conformations of various symmetries were found and examined. The calculated Raman spectra provide support for the conclusion that the S_4 symmetry, at ambient conditions, changes to C_2 under static high-pressure loading and to C_2 or C_1 in solution.

I. Introduction

A good understanding of the microscopic physical and chemical processes that occur in shock wave initiation and detonation of condensed energetic materials is needed for the development of a predictive capability regarding issues of explosive sensitivity, safety, performance, etc. Because typical high explosives are organic molecular solids, the identity of the individual molecules is preserved in the solid.[1] Hence, an understanding of the properties of the molecule, such as its structure, bonding, charge distribution, polarity, and electron affinity, is an important need for characterizing the reactive behavior of explosive molecular solids.

In the present work, we focus on pentaerythritol tetranitrate (PETN; 1,3-propanediol, 2,2-bis(nitroxy)methyl-, dinitrate (ester)). PETN is a crystalline energetic material used extensively as an initiating or booster high explosive. The shock sensitivity of PETN depends strongly on the orientation of the crystal axes relative to the shock propagation direction.[2,3] A mechanistic understanding of this anisotropic behavior is an area of active interest.[4−6] One possible mechanism suggests that the conformation change under shock loading caused by shear deformation may be responsible for the observed anisotropy.[6] Hence, an assessment of the propensity of PETN to conformational changes and characterization of its viable conformers are in order.

As determined by X-ray diffraction measurements, the space group of the PETN crystal is $P\bar{4}2_1c$ and the molecular point group is S_4.[7,8] The structure and vibrational (IR, Raman) spectra of the S_4 conformer were recently analyzed using density functional theory (DFT) methods and were found to agree well with data derived from the crystalline state.[9] However, theoretical or experimental evidence for conformers other than S_4 is lacking. In this work, we use Raman spectroscopy and DFT analyses to observe and examine additional PETN conformers for the first time.

The remainder of this paper is organized as follows. Our approach to the problem and computational and experimental methods used are described briefly in the next section. Section III presents the results of Raman measurements in solution and under static high pressure. Section IV contains computational analyses of the structure and vibrational spectra of several PETN conformers. The results are discussed in section V, and our main findings are summarized in section VI.

II. Approach and Methods

A. Approach. PETN is a flexible molecule that can change its geometry via internal rotations about single bonds; there are 12 such bonds in the molecule, as shown in Figure 1. However, the energy expense associated with such rotations could be several kilocalories per mole, making them energetically unfavorable.[6] Two approaches were utilized in this work to induce a symmetry change in the PETN molecule from the S_4 symmetry, initially adopted in the crystal under ambient conditions.

The first approach takes advantage of the fact that the S_4 conformer is nonpolar; it has no dipole moment due to the high symmetry of the S_4 point group. In a polar solvent, dipole−dipole interactions between the solvent and the solute result in higher solvation energy for polar molecules compared to nonpolar ones.[10] This stabilization may be sufficient for a polar PETN conformer to become the lowest energy conformer. In fact, the dipole moment value of 2.0 D observed previously for PETN in solution[11] could be an indication of such behavior.

The second approach uses static high-pressure compression and the fact that the S_4 conformer occupies nearly the largest volume per molecule compared to other conformers. As the lattice parameters are reduced under static compression, the intermolecular forces increase. This increase may eventually cause a conformation change to minimize the energy of intermolecular repulsion forces through compaction of the molecular geometry. Evidence for torsional angle changes under static high pressure in PETN-d_8 was reported previously in neutron diffraction experiments for pressures up to 4.3 GPa.[12] Also, the rigid-molecule approximation was inadequate for modeling $P-V$ compression data in PETN while it worked well for similar energetic molecular crystals, such as RDX, HMX, and HNIW.[13]

* Corresponding author. E-mail: dreger@wsu.edu.

10.1021/jp040214t CCC: $27.50
Published on Web 06/29/2004

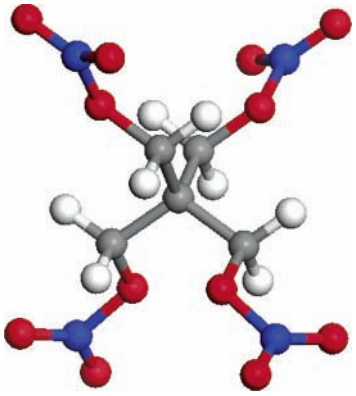

Figure 1. Ball-and-stick model of PETN molecule. Legend: carbon, gray; nitrogen, red; oxygen, blue; hydrogen, white.

Vibrational spectroscopy (Raman and IR) is sensitive to the symmetry of the molecule through selection rules.[14] To observe symmetry changes in PETN in this work, we measure Raman spectra of PETN either in solution or under static high pressure and compare them against the spectrum of PETN single crystal attributed to the S_4 conformer.[9] The observed spectral changes are analyzed and interpreted using computational electronic structure methods.

B. Experimental Methods. The PETN crystals were received from the Los Alamos National Laboratory. The material contained less than 100 ppm organic impurities as indicated by NMR and chromatography. PETN solution in the concentration of 209 mg of PETN/1 g of solvent was prepared using acetone-d_6 (100.0 atom % D, Aldrich).

Static high pressure was generated in a gasketed Merrill-Bassett type diamond anvil cell (DAC) utilizing modified brilliant cut diamonds with 600 μm culets. A small single crystal of PETN (typically 150−200 μm in lateral dimensions and 50−70 μm in thickness) was placed in a 300 μm hole in an Inconel gasket. Glycerol was used as a hydrostatic pressure medium (up to ∼8 GPa). The pressure was determined by monitoring the shift of the R_1 and R_2 fluorescence lines from a small ruby chip. A CW Ar ion laser was used to pump the ruby. Over the range of this study, the R_1 line shifts at a near constant 7.56 cm^{-1} per GPa[15,16] resulting in determination of pressure to a precision of ∼0.05 GPa.

The Raman system consisted of a spectrometer (Spex 500M) equipped with a liquid nitrogen cooled CCD detector (Princeton Instruments). Either the 488.0 nm (solution) line or the 514.5 nm (DAC) line of a CW argon ion laser was used as the excitation source. Holographic notch filters (Kaiser Optical Systems) were employed to reject the excitation light at the input of the spectrometer. Raman data were collected in 90° (solution) and back (DAC) scattering geometries over a frequency range from 400 to 3200 cm^{-1} with a spectral resolution of 1.4 cm^{-1}.

C. Computational Methods. All calculations were performed using the Gaussian 98 suite of quantum chemistry programs.[17] DFT (B3PW91[18,19] and B3LYP[18,20] hybrid functionals) geometry optimizations using the 6-31G(d) basis set[21−25] were carried out to locate stable conformations. The DFT calculations employed the default grid provided by Gaussian 98, which was a pruned (75,302) grid, having 75 radial shells and 302 angular points per shell.[17]

Normal-mode analyses were carried out for the B3PW91/6-31G(d) optimized geometries, and the Raman vibrational spectra were simulated for comparison with experimental data. Spectral lines were simulated by fitting the predicted Raman activities to Lorentzian functions with the full width at half-maximum set to 3 cm^{-1} to mimic the typical line width observed experimentally in crystalline PETN.

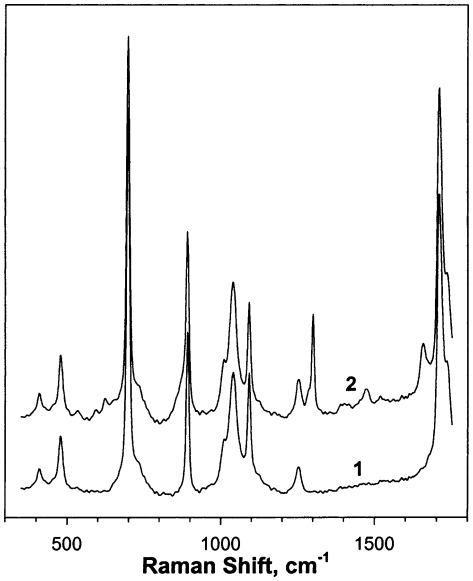

Figure 2. Raman spectra of (1) acetone-d_6 and (2) PETN/acetone-d_6 solution.

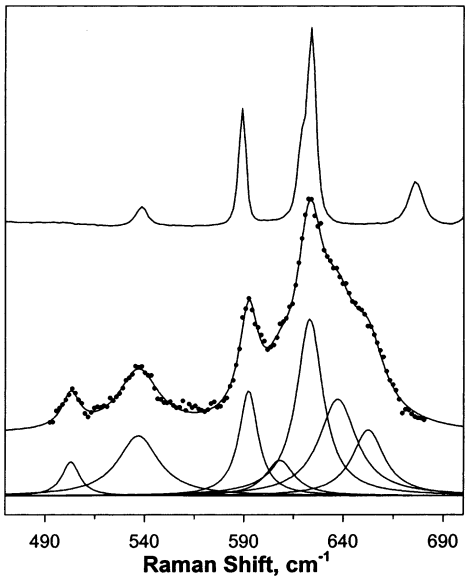

Figure 3. Raman spectra of PETN in the low-frequency range. Top trace: PETN single crystal. Middle trace: PETN dissolved in acetone-d_6. Data points are fitted to a sum of Lorentzians (solid line); the individual Lorentzian peaks used in the fit are shown at the bottom.

III. Experimental Results

A. PETN in Solution. Acetone was chosen as a solvent because it dissolves PETN in very high concentrations[26] necessary for Raman measurements. Also, NMR data indicate that PETN does not form complexes with acetone in solution.[27] Deuterated acetone possesses convenient spectral windows that allow monitoring of symmetry-sensitive PETN modes. As seen in Figure 2, the solvent is transparent (has no Raman modes) from 490 to 680 cm^{-1} and from 1270 to 1680 cm^{-1}. It is also fully transparent in the CH stretching region around 3000 cm^{-1} (not shown).

Figures 3 and 4 compare Raman spectra of PETN in acetone-d_6 and as a single crystal. Besides mode broadening and shifting, which are typical of solutions, several new modes appear that

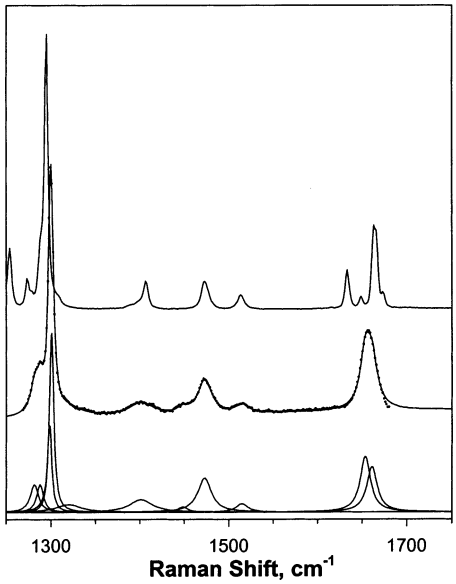

Figure 4. Raman spectra of PETN in the intermediate-frequency range. Top trace: PETN single crystal. Middle trace: PETN dissolved in acetone-d_6. Data points are fitted to a sum of Lorentzians (solid line); the individual Lorentzian peaks used in the fit are shown at the bottom.

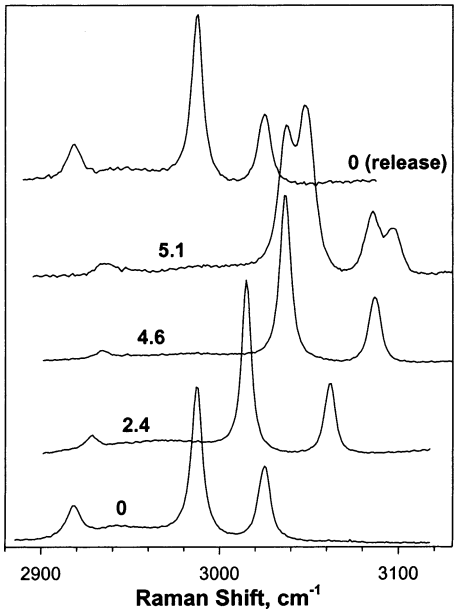

Figure 5. Raman spectra of PETN single crystal under static high-pressure loading in the high-frequency range. Pressure values are shown in gigapascals next to each spectrum.

cannot be assigned a counterpart in the crystal spectrum. In particular, new modes at 503, 637, 652, and 1450 cm^{-1} are well resolved. Some other noticeable changes in the spectrum are (i) the NO_2 antisymmetric stretching modes around 1650 cm^{-1} coalesced into a single band and (ii) the O′N + CC combination stretching mode at 676 cm^{-1} either disappeared or shifted outside the accessible spectral range. Because of the significant mode broadening, no new modes could be discerned in the CH stretching region.

B. DAC Data. Figures 5 and 6 show PETN crystal spectra as a function of pressure. Both figures show that pressure-induced changes up to 5 GPa consist primarily of frequency shifting. However, just above 5 GPa, new features appear in the spectra. In particular, Figure 5 shows that at 5.1 GPa the two stronger CH_2 stretching modes split into doublets. At 5.0 GPa (Figure 6), the strong mode (CCC deformation + ONO_2 rock)[9] initially located at 624 cm^{-1} also splits and develops two shoulders on both the high- and low-frequency sides. These features grow further with pressure. By 5.3 GPa, a group of at least four peaks replaces the initial single peak. All these changes are fully reversible as the spectra revert upon pressure release (see Figures 5 and 6).

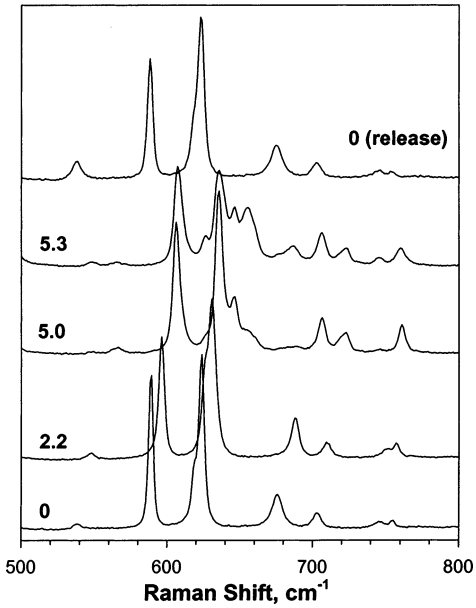

Figure 6. Raman spectra of PETN single crystal under static high-pressure loading in the low-frequency range. Pressure values are shown in gigapascals next to each spectrum.

IV. Computational Results

Because the PETN molecule is *extremely flexible*, there exist numerous stable conformations (local minima on the potential energy surface (PES)). To find all stable conformations, a full PES scan is required. However, because of the 81 degrees of freedom involved, a scan at the DFT level is prohibitively expensive. On the other hand, less extensive semiempirical methods, such as AM1, were found to be unreliable as they often locate minima that do not hold at the DFT level. Also, the relative energy values of the conformers were misleading. To get around this problem, we have limited the search to inspection of a moderate number of representative structures carried out at the B3PW91/6-31G(d) level. Although we have located over 20 stable conformations, this approach may not have provided an exhaustive set of all important low energy structures. Only several representative optimized structures of interest to this work will be presented below. Cartesian atomic coordinates of 11 low energy conformers are given in Table 1S of the Supporting Information.

As reported previously, the global minimum on the PES belongs to the S_4 point group.[6,9] For all practical purposes, the next low energy conformer should be classified as a D_{2d}. The D_{2d} symmetry requires that the two $O_2NOCCCONO_2$ groups of atoms comprising the molecule be strictly planar. Relaxing this requirement reduces the symmetry from D_{2d} to D_2 and expands the number of degrees of freedom from 13 to 21. Although the resulting D_2 conformer lies lower in energy than the D_{2d} by ~0.1 kcal/mol (Table 1), the optimized structures of both are almost identical. The maximum atomic displacement between these two conformers does not exceed 0.028 Å. Stick models of the high-symmetry S_4 and D_{2d} (D_2) conformers are shown in Figure 7.

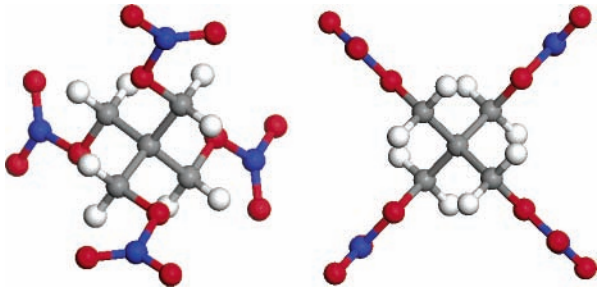

Figure 7. Ball-and-stick models of high-symmetry PETN conformers: S_4 (left); D_{2d} and D_2 (right). Legend is the same as in Figure 1.

TABLE 1: Relative Energies of High-Symmetry Conformers

	energy, kcal/mol		
conformer	B3PW91/ 6-31G(d)	B3LYP/ 6-31G(d)	B3LYP/ 6-311+G(d,p)
S_4	0	0	0
D_{2d}	0.271	0.283	0.339
D_2	0.171	0.200	0.242

Several more optimized structures are shown in Figure 8; their dipole moments and absolute and relative energies are detailed in Table 2. In contrast to the high symmetry conformers that are nonpolar, all conformers of the C_2 and C_1 symmetries have nonzero dipole moments. In the set inspected, the conformer denoted as $C_2(\beta)$ had the largest dipole moment of 5.99 D. To estimate the volume occupied by each structure, we computed the volume inside a contour of 0.001 electron/bohr^3 density. The results are also given in Table 2.

Harmonic vibrational frequencies for the conformers were determined through normal-mode analyses. Each structure has six zero frequencies, and the remaining 81 frequencies are real. All calculated vibrational frequencies, IR intensities, Raman activities, and mode symmetries are listed in Tables 2S and 3S of the Supporting Information. Simulated Raman spectra based upon B3PW91/6-31G(d) calculations are shown in Figures 9 and 10. The vibrational frequencies in Figure 10 have been reduced by 4% from the calculated values; unscaled frequencies are shown in Figure 9.

V. Discussion

Clearly, the applicability of single molecule calculations to a condensed phase is limited. However, as shown in our previous work,[9] DFT methods model well the Raman spectrum of crystalline PETN (S_4 conformer) in the spectral region below 1000 cm^{-1}. This conclusion is reaffirmed in this study and is illustrated by the two bottom traces shown in Figure 9. Good agreement of calculations with experimental data lends a high degree of confidence to DFT treatments of other PETN conformers.

Figure 9 demonstrates the effect of molecular symmetry on the Raman spectrum of PETN in the region from 450 to 800 cm^{-1}. Spectral changes are particularly pronounced between ca. 600 and 700 cm^{-1} when symmetry is lowered from S_4 to C_2 or C_1. To understand this behavior, we note that the initial strong peak at 624 cm^{-1} is in fact a superposition of two overlapped Raman modes: a B mode at 619 cm^{-1} (C_5 skeletal + ONO_2 rock) and an E mode at 624 cm^{-1} (CCC deformation + ONO_2 rock).[9] Symmetry change causes degeneracy lifting for the E mode and frequency shifting for the B mode to produce three separate peaks. Similar changes occur for the next two modes, 676 and 704 cm^{-1}, that are of A and E symmetries, respectively.

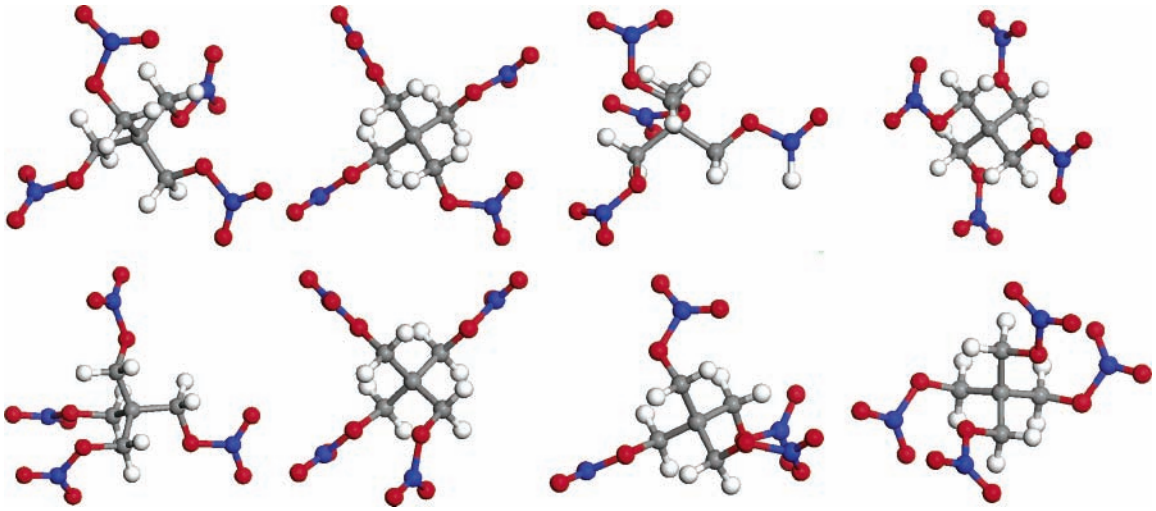

Figure 8. Ball-and-stick models of low-symmetry PETN conformers: $C_1(\alpha)$, $C_1(\beta)$, $C_1(\gamma)$, and $C_2(\alpha)$ (top row from left to right); $C_1(\delta)$, $C_1(\epsilon)$, $C_1(\theta)$, and $C_2(\beta)$ (bottom row from left to right). Legend is the same as in Figure 1.

TABLE 2: Dipole Moments, Absolute and Relative Energies, and Volumes of PETN Conformers

conformer	dipole moment, D	absolute energy, hartrees	zero-point energy, kcal/mol	relative energy,[a] kcal/mol	isodensity volume, cm^3/mol
S_4	0	−1315.981 392 4	120.19	0	191
D_2	0	−1315.981 119 9	120.41	0.39	174
$C_1(\alpha)$	1.06	−1315.979 931 5	120.11	0.84	166
$C_1(\beta)$	1.04	−1315.978 896 0	120.24	1.62	187
$C_1(\gamma)$	1.03	−1315.978 671 0	120.16	1.68	162
$C_2(\alpha)$	1.72	−1315.978 278 8	120.04	1.80	170
$C_1(\delta)$	3.80	−1315.978 259 3	120.18	1.96	170
$C_1(\epsilon)$	3.29	−1315.978 281 5	120.28	2.04	161
$C_1(\theta)$	1.88	−1315.977 939 2	120.15	2.12	192
$C_2(\beta)$	5.99	−1315.975 074 7	120.25	4.03	163

[a] Zero-point-corrected energy relative to S_4.

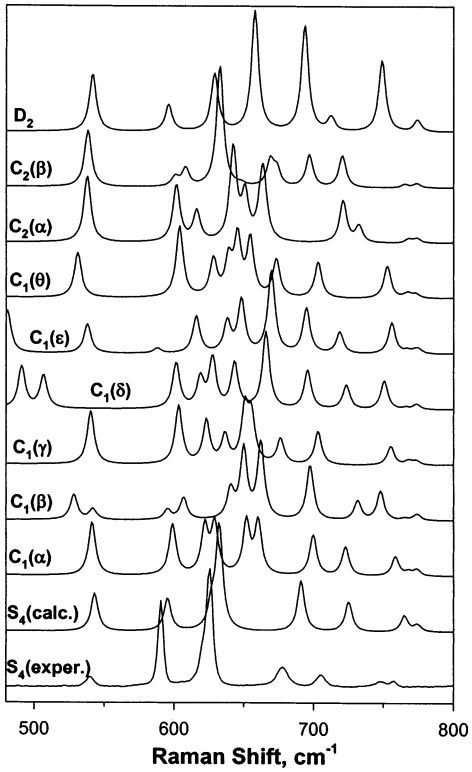

Figure 9. Simulated Raman spectra of PETN conformers in the low-frequency range. Experimental spectrum of PETN single crystal attributed to the S_4 conformer is given for comparison.

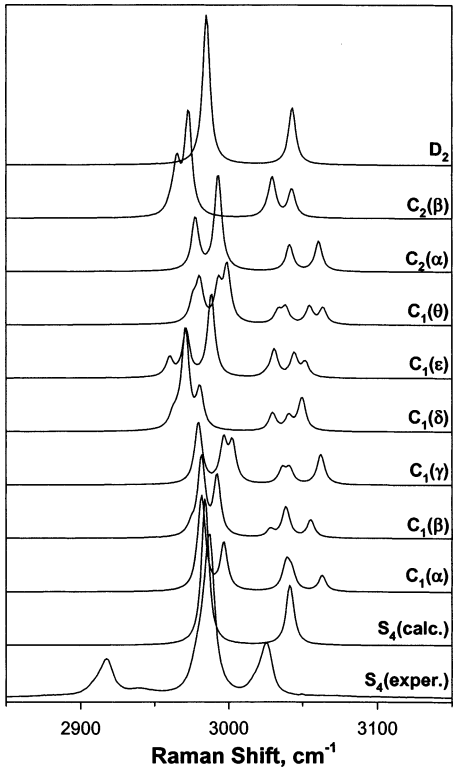

Figure 10. Simulated Raman spectra of PETN conformers in the high-frequency range. The vibrational frequencies used to generate these spectra are reduced by 4%. Experimental spectrum of PETN single crystal attributed to the S_4 conformer is given for comparison.

As a result, the initial three fairly well separated peaks are replaced by a complicated structure of at least six peaks.

The spectra observed experimentally either in solution or in DAC experiments (Figures 3 and 6) are in qualitative agreement with the behavior just indicated. On the basis of this observation, we conclude that in both situations the symmetry of the PETN molecule is likely reduced from S_4 to C_2 or C_1. However, as manifested by the differences in the spectra, the conformer that exists in solution is different from that produced under static high pressure. It is also possible that a mixture of conformers, rather than a single one, is present in solution.

Further information about the probable point group of PETN in the crystal state at pressures above 5 GPa can be obtained from the CH stretching region (Figure 5). As acknowledged previously, [9] DFT modeling is not as accurate for high vibrational frequencies as it is below 1000 cm^{-1} (also, see Figures 9 and 10). Although the calculation correctly predicts the three strong S_4 Raman peaks of B, A, and E symmetry associated with CH_2 stretching modes, the B and E modes appear superimposed in the simulation while they are well apart in the experimental spectrum (see Table 3, Figure 10, and ref 9). Therefore, caution has to be exercised when tracking symmetry-induced changes in this spectral region.

As seen from Table 3, the calculation indicates that upon symmetry change from S_4 to C_2 all three strong peaks tend to split into doublets. For example, in $C_2(\alpha)$, the initial A (2984 cm^{-1}), E (3041 cm^{-1}), and B (3042 cm^{-1}) peaks transform into two A peaks (2977 and 2993 cm^{-1}), two B peaks (3041 and 3061 cm^{-1}), and two A peaks (3041 and 3061 cm^{-1}), respectively. Spectral variations predicted for symmetry change from S_4 to C_1 are significantly more complex and produce combinations of peaks that are less regular than C_2 (Figure 10). The data in Figure 5 show clear splitting of the A and E modes which is consistent with the C_2 symmetry. The diminished intensity of the B mode makes it difficult to track its changes. However, the apparent broadening of the peak at 5.1 GPa could indicate the splitting of the B mode as well.

Additional support for the symmetry change conclusion, under high pressure, to C_2 rather than to C_1 comes from the comparison of the calculated C_2 spectra in the low-frequency region (Figure 9) with experimental data (Figure 6). In particular, the spectrum of $C_2(\alpha)$ is very similar to the experimental spectrum detected at 5.3 GPa. To summarize, both high- and low-frequency spectra offer strong support for the conclusion that the symmetry changes from S_4 to C_2 in PETN crystal under static high-pressure

TABLE 3: CH Stretching Modes of PETN Conformers[a]

	S_4				$C_2(\alpha)$			$C_2(\beta)$		
mode no.	freq (exptl)	freq	Raman act.	sym	freq	Raman act.	sym	freq	Raman act.	sym
74		2982	0.1	B	2977	9.8	B	2960	15.4	B
75	2940	2983	16.9	E	2977	88.6	A	2965	92.8	A
76					2992	18.4	B	2971	19.3	B
77	2987	2984	262.9	A	2993	164.5	A	2973	179.1	A
78		3040	0.1	A	3041	27.1	B	3025	6.6	A
79	3025	3041	72.8	E	3041	23.0	A	3030	74.5	B
80					3061	28.4	A	3042	19.5	B
81	2918	3042	49.2	B	3061	29.4	B	3043	34.3	A

[a] Frequency in cm^{-1} (calculated vibrational frequencies have been reduced by 4%); Raman activities in $Å^4$/amu.

loading. The $C_2(\alpha)$ conformer is the most probable structure of PETN above 5 GPa. The C_2 symmetry is not compatible with the $P\bar{4}2_1c$ tetragonal space group of the PETN crystal under ambient conditions. Therefore, the symmetry change from S_4 to C_2 constitutes a solid−solid phase transition in PETN. The most probable space group of the new phase is the $P2_12_12$ orthorhombic. More detailed high-pressure results with the analysis of both point and space group changes in the PETN crystal lattice will be presented in a future paper.

Furthermore, the isodensity volume values presented in Table 2 offer an insight into the force driving the conformation change under compression. As seen in Table 2, among PETN conformers, the S_4 conformer occupies nearly the largest volume per molecule. On average, low-symmetry conformers take up ca. 10% less space than S_4 and $C_2(\alpha)$ is 11% more compact. As discussed in previous studies,[13,28] the initial compression of an organic molecular crystal is almost entirely due to a reduction of intermolecular distances. However, at higher compressions, the increase of van der Waals repulsions becomes comparable with the intramolecular repulsion forces that control molecular geometry. Because the $C_2(\alpha)$ conformer is more compact, it will produce less intermolecular repulsion energy in the crystal. When this energy gain exceeds the energy gap between S_4 and $C_2(\alpha)$, PETN molecules will be forced to change conformation. We believe that this mechanism is likely responsible for the transition observed in the crystal above 5 GPa.

VI. Summary

The Raman measurements and DFT calculations presented here have provided insight into the susceptibility of PETN to conformational changes. The primary conclusions are as follows: The PETN molecule is extremely flexible and can exist in the form of various conformers that differ in energy, symmetry, polarity, etc. The molecular environment and physical conditions control the conformation that the PETN molecule adopts. Change of conformation/symmetry can be readily observed through changes in the vibrational spectrum.

In the crystalline phase under ambient conditions, the PETN molecule has S_4 symmetry. Two instances of symmetry change from S_4 to lower symmetry were found and presented in this work. One involved compressing the PETN crystal statically to ≥ 5 GPa in a diamond anvil cell. The other was observed upon dissolving PETN in a polar solvent (acetone-d_6).

DFT single molecule calculations were carried out to assess and interpret the changes observed experimentally in the Raman spectra. Several representative stable PETN conformations of various symmetries (S_4, D_{2d}, D_2, C_2, and C_1) were found and examined. The calculated Raman spectra provided support for the conclusion of a symmetry change from S_4 to C_2 in crystalline PETN under static high-pressure loading and to C_2 or C_1 in solution. It is possible that a mixture of conformers, rather than a single one, is present in solution.

Acknowledgment. We thank Dr. J. J. Dick for providing PETN samples and for many stimulating discussions during the early stages of this project. Calculations were performed on the HP/Convex Exemplar SPP-2000 supercomputer at the National Center for Supercomputing Applications (NCSA) of the University of Illinois at Urbana−Champaign. The authors gratefully acknowledge the NCSA for the allotment of computer time under Grant DMR990014N. This work was supported in part by ONR Grant N00014-01-1-0802 and DOE Grant DEFG0397SF21388.

Supporting Information Available: Atomic coordinates for the optimized structures; vibrational frequencies, IR intensities, Raman activities, and mode symmetries calculated at the B3PW91/6-31G(d) level. This material is available free of charge via the Internet at http://pubs.acs.org.

References and Notes

(1) Galwey, A. K. *Chemistry of Solids*; Chapman and Hall: London, 1967.
(2) Dick, J. J. *Appl. Phys. Lett.* **1984**, *44*, 859.
(3) Dick, J. J.; Mulford, R. N.; Spencer, W. J.; Pettit, D. R.; Garcia, E.; Shaw, D. C. *J. Appl. Phys.* **1991**, *70*, 3572.
(4) Dick, J. J.; Ritchie, J. P. *J. Appl. Phys.* **1994**, *76*, 2726.
(5) Jindal, V. K.; Dlott, D. D. *J. Appl. Phys.* **1998**, *83*, 5203.
(6) Gruzdkov, Y. A.; Gupta, Y. M. *J. Phys. Chem. A* **2000**, *104*, 11169.
(7) Cady, H. H.; Larson, A. C. *Acta Crystallogr., Sect. B* **1975**, *B31*, 1864.
(8) Conant, J. W.; Cady, H. H.; Ryan, R. R.; Yarnell, J. L.; Newsam, J. M. Informal Report LA-7756-MS; Los Alamos National Laboratory: Los Alamos, NM, 1979.
(9) Gruzdkov, Y. A.; Gupta, Y. M. *J. Phys. Chem. A* **2001**, *105*, 6197.
(10) *Solute-Solvent Interactions*; Coetzee, J. F., Ritchie, C. D., Eds.; Marcel Dekker: New York, 1969.
(11) Smyth, C. P. *Dielectric Behavior and Structure*; McGraw-Hill: New York, 1955; p 288.
(12) Dick, J. J.; von Dreele, R. B. In *Shock Compression of Condensed Matter—1997*; Schmidt, S. C., Dandekar, D. P., Forbes, J. W., Eds.; American Institute of Physics: Woodbury, NY, 1998; p 827.
(13) Sorescu, D. C.; Rice, B. M.; Thompson, D. L. *J. Phys. Chem. B* **1999**, *103*, 6783.
(14) Cotton, F. A. *Chemical Applications of Group Theory*; Wiley: New York, 1990.
(15) Piermarini, G. J.; Block, S.; Barnett, J. D.; Forman, R. A. *J. Appl. Phys.* **1975**, *46*, 2774.
(16) Barnett, J. D.; Block, S.; Piermarini, G. J. *Rev. Sci. Instrum.* **1973**, *44*, 1.
(17) Frisch, M. J.; Trucks, G. W.; Schlegel, H. B.; Scuseria, G. E.; Robb, M. A.; Cheeseman, J. R.; Zakrzewski, V. G.; Montgomery, Jr., J. A.; Stratmann, R. E.; Burant, J. C.; Dapprich, S.; Millam, J. M.; Daniels, A. D.; Kudin, K. N.; Strain, M. C.; Farkas, O.; Tomasi, J.; Barone, V.; Cossi, M.; Cammi, R.; Mennucci, B.; Pomelli, C.; Adamo, C.; Clifford, S.; Ochterski, J.; Petersson, G. A.; Ayala, P. Y.; Cui, Q.; Morokuma, K.; Malick, D. K.; Rabuck, A. D.; Raghavachari, K.; Foresman, J. B.; Cioslowski, J.; Ortiz, J. V.; Baboul, A. G.; Stefanov, B. B.; Liu, G.; Liashenko, A.; Piskorz, P.; Komaromi, I.; Gomperts, R.; Martin, R. L.; Fox, D. J.; Keith, T.; Al-Laham, M. A.; Peng, C. Y.; Nanayakkara, A.; Gonzalez, C.; Challacombe, M.; Gill, P. M. W.; Johnson, B.; Chen, W.; Wong, M. W.; Andres, J. L.; Gonzalez, C., Head-Gordon, M.; Replogle, E. S.; Pople, J. A. *Gaussian 98*, Revision A.7; Gaussian, Inc.: Pittsburgh, PA, 1998.
(18) Lee, C.; Yang, W.; Parr, R. G. *Phys. Rev. B* **1988**, *37*, 785.
(19) Burke, K.; Perdew, J. P.; Wang, Y. In *Electronic Density Functional Theory: Recent Progress and New Directions*; Dobson, J. F., Vignale, G., Das, M. P., Eds.; Plenum Press: London, 1998.
(20) Becke, A. D. *J. Chem. Phys.* **1993**, *98*, 5648.
(21) Hehre, W. J.; Ditchfield, R.; Pople, J. A. *J. Chem. Phys.* **1972**, *56*, 2257.
(22) Hariharan, P. C.; Pople, J. A. *Theor. Chim. Acta* **1973**, *28*, 213.
(23) Gordon, M. S. *Chem. Phys. Lett.* **1980**, *76*, 163.
(24) McLean, A. D.; Chandler, G. S. *J. Chem. Phys.* **1980**, *72*, 5639.
(25) Krishnan, R.; Binkley, J. S.; Seeger, R.; Pople, J. A. *J. Chem. Phys.* **1980**, *72*, 650.
(26) Urbanski, T. *Chemistry and Technology of Explosives*; Pergamon Press: Oxford, 1965; Vol. II, p 178.
(27) Binks, P. R.; French, C. E.; Nicklin, S.; Bruce, N. C. *Appl. Environ. Microbiol.* **1996**, *62*, 1214.
(28) Pastine, D. J.; Bernecker, R. R. *J. Appl. Phys.* **1974**, *45*, 4458.